Submitted to PCCP, xx/xx/2022

Acetylene hydrogenation catalyzed by bare and Ni doped CeO_2(110): The role of frustrated Lewis pairs

Shulan Zhou,[1,2] * Qiang Wan,[3] Sen Lin,[3,*] and Hua Guo[2]

[1]*School of Chemistry and Chemical Engineering, Shandong University of Technology, Zibo 255000, China*

[2]*Department of Chemistry and Chemical Biology, University of New Mexico, Albuquerque, New Mexico 87131, USA*

[3]*State Key Laboratory of Photocatalysis on Energy and Environment, College of Chemistry, Fuzhou University, Fuzhou 350002, China*

*Corresponding authors. Email: zhoushulan2009@126.com and slin@fzu.edu.cn

Abstract

Ceria (CeO_2) has recently been found to catalyze the selective hydrogenation of alkynes, which has stimulated much discussion on the catalytic mechanism on various facets of the reducible oxide. In this work, the H_2 dissociation and acetylene hydrogenation on bare and Ni doped $CeO_2(110)$ surfaces are investigated using density functional theory (DFT). Similar to that on the $CeO_2(111)$ surface, our results suggest that the catalysis is facilitated by frustrated Lewis pairs (FLPs) formed by oxygen vacancies (O_vs) on the oxide surfaces. On bare $CeO_2(110)$ with a single O_v ($CeO_2(110)$-O_v), two surface Ce cations with one non-adjacent O anion are shown to form (Ce^{3+}-Ce^{4+})/O quasi-FLPs, while for the Ni doped $CeO_2(110)$ surface with one (Ni-$CeO_2(110)$-O_v) or two (Ni-$CeO_2(110)$-$2O_v$) O_vs, one Ce and a non-adjacent O counterions are found to form a mono-Ce/O FLP. DFT calculations indicate that Ce/O FLPs facilitate the H_2 dissociation via a heterolytic mechanism, while the resulting surface O-H and Ce-H species catalyze the subsequent acetylene hydrogenation. With $CeO_2(110)$-O_v and Ni-$CeO_2(110)$-$2O_v$, our DFT calculations suggest the first hydrogenation step is the rate-determining step with a barrier of 0.43 and 0.40 eV, respectively. For Ni-$CeO_2(110)$-O_v, the reaction is shown to be controlled by the H_2 dissociation with a barrier of 0.41 eV. These barriers are significantly lower than that (about 0.7 eV) on $CeO_2(111)$, explaining the experimentally observed higher catalytic efficiency of the (110) facet of ceria. The change of rate-determining step is attributed to the different electronic properties of Ce in the Ce/O FLPs – the Ce *f* states closer to Fermi level facilitate the heterolytic dissociation of H_2 but also leads to the higher barrier of acetylene hydrogenation.

Key words: acetylene hydrogenation; oxygen vacancy; Ni doped $CeO_2(110)$; frustrated Lewis pairs

1. Introduction

The selective hydrogenation of alkynes to alkenes is an important step in alkenes polymerization, as acetylenic impurities from steam cracking of crude oil can poison the polymerization catalysts.[1] Although Pd catalysts are commonly used for this purpose,[2-4] they suffer from low selectivity due to over-hydrogenation and oligomerization.[1, 4, 5] Furthermore, the scarcity of the precious metal has become exacerbated recently because of high demand and limited supply. As a result, searching for alternative cost-effective catalysts for selective alkyne hydrogeneration has attracted considerable recent interest.

Recently, ceria (CeO_2) has emerged as a surprising catalyst for selective hydrogenation reactions.[6-17] This oxide is an attractive substitution of the Pd catalysts because it is abundant and relatively inexpensive. In 2012, Vilé et al. reported for the first time that CeO_2 is a highly selective catalyst for the partial hydrogenation of propyne and ethyne.[12] However, its practical application was somewhat limited by the high reaction temperature (above 500 K) required for its activity. This discovery has since stimulated several mechanistic investigations aimed at a better understanding of the hydrogenation mechanism on CeO_2,[18-23] which could help the design of more effective catalysts. In 2014, Carrasco et al. proposed a mechanism based on density functional theory (DFT), which suggested that C_2H_2 on $CeO_2(111)$ is hydrogenated by surface O-H groups generated by the homolytic H_2 dissociation.[18] However, the calculated barrier of the second hydrogenation step (C_2H_3* + H* → C_2H_4) is as high as 2.86 eV, rendering this mechanism unrealistic. Also based on DFT, some of current authors proposed more recently a different mechanism based on surface oxygen vacancies (O_vs) on $CeO_2(111)$, which promote heterolytic H_2 dissociation. [23] Specifically, the resulting Ce and O near the O_v help to form frustrated Lewis pairs (FLPs), which are spatially non-contacting acid-base pairs,[24, 25] on the catalytic surface.[11, 19, 23]

Such surface FLPs have been shown to activation of small molecules, such as CO_2 and H_2.[26-31] The Ce cations exposed by O_vs play a vital role in the lowering of reaction barrier, by not only stabilizing the Ce-H hydride but also avoiding the strong adsorption of intermediate C_2H_3. The calculated rate-determining barrier in the new mechanism is 0.70 eV, which is significantly lower than that (2.86 eV) of the mechanism proposed by Carrasco et al.[18] This new mechanism was further supported by the observation of Ce-H hydrides in neutron scattering experiment,[32] which are absent in the mechanism of Carrasco et al.,[18] and was also corroborated by electron spin resonance and electron energy loss spectroscopy spectroscopic signatures.[33, 34] More recently, the involvement of surface hydrides in acetylene hydrogenation on reduced ceria was further confirmed by the *in situ* inelastic neutron scattering spectroscopy,[6] providing definitive evidence for our hydrogenation mechanism based on H_2 heterolytic dissociation.

Moreover, metal doping seems to enhance the activity of the ceria catalyst in selective hydrogenation. For example, Ga was introduced into CeO_2 by the Pérez-Ramírez group to lower the reaction temperature of the catalyzed acetylene hydrogenation.[20] Theoretically, this was attributed to Ga/O FLPs induced by O_vs on Ga doped CeO_2(111), which facilitate in the heterolytic dissociation of H_2 and the subsequent hydrogenation step.[22] To increase the catalytic efficiency of CeO_2, a new catalyst design based Ni doping was proposed to promote the formation of O_vs on CeO_2(111) surfaces, which was confirmed by experiment.[23] In this case, the Ni dopant was not directly involved in the FLP-facilitated catalysis, but served as a single atom promoter for the formation of oxygen vacancies. The vital role of O_vs in hydrogenation reactions was also found on several other oxides, including the tungsten oxide, indium oxide, bimetal oxide, and titanium dioxide.[35-39]

It is well established that the catalytic activity of ceria is facet dependent.[11, 13, 14, 40-46] For example, the heterolytic dissociation of H_2 on stoichiometric $CeO_2(110)$ is easier than on the $CeO_2(111)$ counterpart and the stability of the hydride species is related to the coordination number of Ce on various CeO_2 surface such as $CeO_2(221)$, $CeO_2(223)$, $CeO_2(132)$, etc.[19, 45-47] Vilé et al.[13] reported that $CeO_2(111)$ was more active than $CeO_2(100)$ for acetylene hydrogenation. Chang and coauthors found that $CeO_2(110)$ and $CeO_2(100)$ with O_vs are efficient catalysts for hydrogenation of alkenes and alkynes.[11, 19] More recently, Cao et al. reported that CeO_2 rod dominated by the (110) facet show the highest catalytic performance for acetylene hydrogenation among all ceria facets.[14] On $CeO_2(110)$, again, the regulated O_vs were believed to lead to the formation of the Ce/O FLPs, which promote the H_2 heterolytic dissociation with a small barrier and leads to a much lower rate-determining barrier (0.58 eV) for acetylene hydrogenation.[19] In this work, we extend our theoretical investigation on ceria based hydrogenation catalysis to a different facet of the CeO_2 surface ($CeO_2(110)$). We further study the impact of metal doping, which is expected to promote the formation of O_vs on $CeO_2(110)$.[48-53] To facilitate the comparison with the results based on $CeO_2(111)$,[23] the adsorption and reaction properties of H_2 and C_2H_2 on bare and Ni doped $CeO_2(110)$ model surfaces with O_vs are calculated by using DFT. The results suggest that the catalytic mechanism on the (110) facet of ceria is similar to that on the (111) facet, but with a lower overall barrier, consistent with previous theory[19] and in good agreement with experimental observations.[14] Furthermore, our calculations suggest that Ni doping on $CeO_2(110)$ helps the formation of the O_vs on the surface which induces a mono-Ce/O FLP to facilitate the H_2 dissociation and C_2H_2 hydrogenation. This publication is organized as follows: Section II provides the computational details. The calculated results and discussions are presented in Section III. The conclusions are discussed in the final section.

2. Computational details

All calculations were performed with spin-polarized DFT as implemented in Vienna Ab initio Simulation Package (VASP).[54, 55] The exchange-correlation potential was treated by the Perdew-Burke-Ernzerhof (PBE) gradient-corrected approximation.[56] The van der Waals correction was included using the DFT-D3 method of Grimme.[57] The wave functions for the valence electrons were expanded in plane waves up to a cutoff energy of 400 eV, while the core electrons were described by projector augmented-wave (PAW) method.[58] In order to properly describe the behavior of Ce *f* electrons, the DFT+*U* method with an effective *U* of 4.5 eV was used.[59-61] The CeO_2(110) surface was modeled by a $p(2 \times 3)$ five-atomic-layer supercell with the bottom two layers fixed while the other layers fully relaxed. For Ni doped CeO_2, a surface Ce was substituted by a Ni. A vacuum space of 14 Å was employed between the neighboring interleaved slabs. A 1×1×1 and a 5×5×1 Monkhorst-Pack mesh *k*-points for relaxation and calculations of electronic properties, respectively. The dipole correction was employed in all calculations. The parameters were tested for convergence.

Transition states (TSs) were determined using the climbing image nudged elastic band (CI-NEB) method,[62] with no spin constrained. All structures were relaxed with the convergence criteria of 0.05 eV/Å and 10^{-4} eV for forces on each ion and for energy, respectively, while for electronic properties, the criterium was increased to 10^{-6} eV for energy. The adsorption energy of a pertinent species was computed as follows: $E_{ads} = E_{(adsorbate + surface)} - E_{(free\ molecule)} - E_{(free\ surface)}$. The reaction energy ($\Delta E$) is given by the energy difference between an initial state (IS) and a final state (FS), and the activation energy (E_a) was calculated by the energy difference between IS and TS. The formation energy of an O_v was obtained by the following equation: $E_f = E(\text{surface-}O_v) + 1/2E(O_2) -$

E(surface), while the formation energy of a second O_v was calculated using the equation E_f=E(surface-2O_v)+1/2E(O_2) –E(surface-O_v).

The metal cations on the surface of the oxide can be considered as a Lewis acid because of their ability to accept electrons, while the oxygen anions on the same surface behave as a Lewis base. If the acid and base are adjacent to each other within a bonding distance (1-2 Å), they are often considered as a classical Lewis pair (CLP). However, if the combination of the Lewis pair is sterically encumbered with the distance between them being more than about 2 Å, [19] they are qualified as an FLP.[24, 25, 28, 63] CLPs are typically less active than FLP in catalysis since FLPs are essential in creating a local environment that is conducive to catalysis.[64]

3. Results and discussion

3.1 Models for bare and Ni doped CeO_2(110) surfaces

The optimized geometries of the CeO_2(110) and Ni doped CeO_2(110) surfaces are shown in Figure 1. For CeO_2(110) (Figure 1(a)), the calculated formation energy of an O_v is 1.73 eV, which is much lower than that (2.57 eV) of CeO_2(111),[23] indicating that CeO_2(110) is easier to be reduced than CeO_2(111). This is consistent with previous studies.[49] To keep the charge balance, two Ce^{4+} need be reduced to Ce^{3+} after removing one surface oxygen. Since the position of Ce^{3+} can affect the energy, several configurations with Ce^{3+} at different positions were considered (Figure S1). It was found that the configuration with Ce^{3+} located at the one surface 5-coordinated Ce (Ce1 in Figure S1 (a)) and one 6-coordinated Ce (Ce3 in Figure S1 (a)) is the most stable one, which was thus used in this work. In this configuration, the Ce1-O1 and Ce2-O1 distances are more than 4.4 Å, satisfying the criteria for a potential FLP. As indicated in Figure S1 (a), the oxidation state of Ce1 (Ce2) is +3 (+4). O2 is in the middle of two Ce atoms (see Figure 2 (b)),

resulting in Ce1/Ce2 surrounded by three oxygens. The electronic interaction between these oxygens and Ce1/Ce2 would potentially hinder the activation of adsorbates by the FLP.[11] Thus, the potential FLP is denoted as (Ce^{3+}-Ce^{4+})/O quasi-FLP, which is expected to be less efficient than the FLP created by removing two oxygens of CeO_2(110) as that proposed in the previous DFT studies by Chang and coauthors.[11, 19] The removal of O2 will lead to two Ce^{3+}, which is denoted as the bi-Ce^{3+}/O FLP. However, the formation of a single O_v in the unit cell is much easier than two such vacancies since the formation energy of the second O_v (2.31 eV) is much larger than that of the first O_v, (1.73 eV). Therefore, in this work, the model of CeO_2(110) with one O_v (CeO_2(110)-O_v, Figure 1(b)) was considered.

On Ni doped CeO_2(110) (Figure 1 (c)), a Ce was replaced by the Ni dopant, which forms a square planar configuration by binding to two surface O atoms and two subsurface ones. This leads to a large distortion of surface structure, resulting in two unstable 2-fold oxygen atoms. Removing one of the 2-fold O is thermally favorable with an exothermicity of –0.59 eV, which is consistent with the values of -0.24 and -0.68 eV calculated by Nolan [51] and Li et al,[53] respectively. The exothermicity suggests a likely spontaneous formation of an O_v. This is very similar to the situation of Ni doped CeO_2(111).[23] The formation of this O_v leads to one 5-coordinated surface Ce and one 7-coordinated subsurface Ce. Comparing the structure of Ni doped CeO_2(110) with one O_v (Ni-CeO_2(110)-O_v) (Figure 1 (d)) with that of CeO_2(110)-O_v, it is found that the substitution of Ce2 by Ni makes only one Ce (Ce1) with the nonadjacent O1 form a potential FLP. To understand the valence state of Ce in Ni-CeO_2(110)-O_v, the spin density of Ni-CeO_2(110)-O_v was calculated (Figure S2). No spin density was observed on Ce atoms, suggesting that the transition of $Ce^{4+}\rightarrow Ce^{3+}$ does not occur in Ni-CeO_2(110)-O_v. It might be due to the fact that the charge imbalance caused by Ni^{2+} substituting Ce^{4+} can be compensated by an O_v. Therefore, the

Ce1/O1 FLP is denoted as mono-Ce^{4+}/O FLP. For Ni and O2, the Ni-O2 distance is 3.52 Å, which also satisfies the criteria for an FLP (denoted as Ni/O FLP). On the other hand, the adjacent Ce1 and O2 can be seen as a CLP (denoted as Ce1/O2 CLP). These Lewis pairs might play a role in C_2H_2 hydrogenation. The model of Ni-CeO_2(110)-O_v was used to study the mechanism of C_2H_2 hydrogenation on Ni doped CeO_2.

The formation of a second O_v on Ni-CeO_2(110)-O_v can lead to two Ce^{3+}, showing a similar degree of reduction to that of CeO_2(110)-O_v. Furthermore, the formation of a second O_v by removing O1, O2 or O3 was also studied. The optimized geometries are shown in Figure S3. The calculated formation energy of the second O_v is 1.91, 1.49 and 2.00 eV for O1, O2 and O3, respectively, indicating O2 is easier to be removed than O1 and O3. For the second O_v formed by O2, several configurations with different Ce^{3+} locations were calculated and are shown in Figure S4. Configuration (a) is the most stable one and was used in this work (Figure 1 (e)), which is consistent with the previous results.[51] The formation energy of 1.49 eV is also very close to the value of 1.30 eV calculated by Nolan[51] and is lower than that (1.73 eV) of the first O_v on bare CeO_2(110), indicating again that Ni doping increases the reductivity of CeO_2(110). As indicated in Figure 1 (e), the removal of O2 makes Ce1 4-coordinated and reduced to +3, with a Ce1-O1 distance of 4.54 Å, forming an FLP denoted as mono-Ce^{3+}/O FLP. In order to study the effect of Ce on the C_2H_2 hydrogenation, the model with two O_vs (denoted as Ni-CeO_2(110)-2O_v) was also considered in this work.

3.2 H_2 dissociation on bare and Ni doped CeO_2(110)

For CeO_2(110)-O_v, the Ce sites and O in green circles form a (Ce^{3+}-Ce^{4+})/O quasi-FLP (see Figure 1 (b)). To investigate its activity, the dissociation of H_2 on (Ce^{3+}-Ce^{4+})/O quasi-FLP via a heterolytic path was calculated. (The calculated barrier for homolytic dissociation is much higher

(1.21 eV) and thus not discussed here.) The calculated energetics is given in Table 1 and the corresponding geometries of H_2 dissociation are shown in Figure 2(a)-(c).

Before dissociation, H_2 weakly adsorbs on the O_v site with an adsorption energy of –0.27 eV and an H-H distance of 0.75 Å, consistent with the geometry calculated by Zhang et al.[11] who did not study the dissociation of H_2 on $CeO_2(110)$-O_v. In the TS, the H-H distance increases to 0.93 Å, while the O1-H2, Ce1-H1, and Ce2-H1 distances decrease to 1.41, 2.91, and 2.74 Å, respectively. The cleavage of the H-H bond needs to overcome a barrier of 0.12 eV, which is significantly lower than that (0.55 eV[19], 0.45 eV[45]) on the CLP of the defect-free $CeO_2(110)$, and is very close to that (0.07 eV)[11, 19] on the bi-Ce^{3+}/O FLP of $CeO_2(110)$-$2O_v$, implying that (Ce^{3+}-Ce^{4+})/O quasi-FLP promotes H_2 dissociation. Moreover, the barrier is 0.40 eV lower than that (0.52 eV)[23] on $CeO_2(111)$-O_v, suggesting that $CeO_2(110)$-O_v is more active than $CeO_2(111)$-O_v for H_2 dissociation. After the reaction, the H_2 breaks into an O-H and a Ce-H hydride. During the dissociation process, O2 moves away from the bridge site formed by the Ce^{3+}-Ce^{4+}, suggesting that the transformation of the (Ce^{3+}-Ce^{4+})/O quasi-FLP to a more efficient (Ce^{3+}-Ce^{4+})/O FLP is relatively easy. This is consistent with the discussion of dynamic FLPs on CeO_2 by Huang et al.[65] To conclude, the (Ce^{3+}-Ce^{4+})/O quasi-FLP shows high activity for H_2 dissociation.

On Ni-$CeO_2(110)$-O_v, there are two potential FLPs, namely the Ni/O FLP and mono-Ce^{4+}/O FLP. On the other hand, there is also a Ce1/O2 CLP. Our calculations indicated that the adsorption of H on the square planar Ni is not stable which migrated to the neighboring 2-fold O site during optimization, implying that the Ni/O FLP is inactive. Thus, H_2 dissociation on the Ni/O FLP was not considered. To understand the activity of these sites, H_2 dissociation on mono-Ce^{4+}/O FLP (Path I) and Ce1/O2 CLP (Path II) was studied. The reaction and activation energies of Path I are given in Table 1. The related geometries for stationary points in Path I and Path II are shown in

Figure 2 (f)-(h) and Figure S5 (a)-(c), respectively. For both paths, H_2 firstly adsorbed on the O_v site with the adsorption energy of –0.21 eV and –0.23 eV, respectively. Along Path I, the TS (Figure 2(g)) is stabilized by O1 and Ce1 with the distances of 1.28, 2.54 and 0.99 Å for the O2-H1, Ce1-H2 and H1-H2 pairs, respectively. The dissociation results in the O-H and Ce-H species by surpassing a barrier of 0.41 eV with an endothermicity of 0.21 eV. For Path II, the TS is also stabilized by Ce1 and O1 and the activation barrier of 0.54 eV, which is 0.13 eV higher than that (0.41 eV) of Path I, suggests that the mono-Ce^{4+}/O FLP is more active than Ce1/O2 CLP. At the TS (Figure S5 (b)), the H-H distance extends to 1.02 Å with the O1-H1, Ce1-H1 and Ce1-H2 distances reduced to 1.27, 2.28 and 2.45 Å, respectively. In the final state (Figure S5 (c)), H_2 dissociates into O-H and Ce-H with an endothermicity of 0.04 eV. On Ni-CeO_2(110)-O_v, hence, our results suggest that H_2 prefers to dissociate via Path I. The barrier (0.41 eV) of this path is 0.29 eV higher than that on CeO_2(110)-O_v, but is about 0.1 eV lower than that (0.50 eV)[23] on Ni-CeO_2(111)-O_v and lower than that of the heterolytic dissociation on o-terminated step site of CeO_2(111) (0.48 to 0.73 eV),[45 46] showing the efficiency of Ni-CeO_2(110)-O_v.

On Ni-CeO_2(110)-$2O_v$, the Ni/O FLP formed by Ni and O2 is absent due to the removal of O2. The possibility of H_2 dissociation on Ni/O3 was firstly studied. The optimized geometries of H_2 adsorption and dissociation product (H-Ni + H-O) are displayed in Figure S6. However, when the adsorbed H_2 and the dissociation product as the IS and FS states of the CI-NEB calculations were used to search for the transition state, it found that H_2 prefers to dissociate into H-O and H-Ce (The geometry is shown in Figure 2 (m)) rather than form H-Ni and H-O (Figure S6 (b). Therefore, only H_2 dissociation on the mono-Ce^{3+}/O FLP was studied. The related geometries and the reaction/activation energies are given in Figure 2 (k)-(m) and Table 1, respectively. The H_2 dissociation on Ni-CeO_2(110)-$2O_v$ is similar to that on Ni-CeO_2(110)-O_v. As shown in Figure 2

(k)-(m), the weakly adsorbed H_2 (–0.22 eV) dissociates into Ce-H and O-H groups via a heterolytic path. At the TS, the distance of H-H is increased to 0.98 Å, while the Ce1-H and O1-H distances are reduced to 2.58 and 1.31 Å, respectively, underscoring the role of the mono-Ce^{3+}/O FLP in the stabilization of the TS. The calculated barrier of H_2 dissociation is 0.13 eV, about 0.28 eV lower than that on mono-Ce^{4+}/O FLP and very close to that (0.12 eV) on the (Ce^{3+}-Ce^{4+})/O quasi-FLP of $CeO_2(110)$-O_v, suggesting that the reduction of Ce from +4 to +3 states enhances the activity of the mono-Ce/O FLP for H_2 dissociation. Moreover, the barrier (0.13 eV) is much lower than that of the heterolytic dissociation of H_2 on the step sites of $CeO_2(111)$ (0.48 to 0.73 eV),[46] showing Ni-$CeO_2(110)$-$2O_v$ is effective for H_2 dissociation.

The stability of the Ce-H hydride resulted from H_2 dissociation is quite important for the subsequent C_2H_2 hydrogenation, so that the migration of the hydride on $CeO_2(110)$-O_v, Ni-$CeO_2(110)$-O_v and Ni-$CeO_2(110)$-$2O_v$ were investigated. The corresponding geometries are shown in Figure 2 (c)-(e), (h)-(j) and (m)-(o), respectively, and the reaction and activation energies are listed in Table 1. On $CeO_2(110)$-O_v, the H migration from Ce to neighbor O needs to overcome a barrier of 1.06 eV, confirming its stability. On Ni-$CeO_2(110)$-O_v, the migration barrier is 0.73 eV, implying that the Ce-H hydride is also quite stable. On Ni-$CeO_2(110)$-$2O_v$, the barrier is 1.14 eV, again indicating the high stability of Ce-H hydride. In addition, these barriers (0.73 and 1.14 eV) are much higher than those of the low-coordinated Ce hydride migration (0 to 0.55 eV)[46] on the step sites of $CeO_2(111)$. Based on these results, we thus conclude that the hydride formed by heterolytic dissociation of H_2 is stable and the subsequent C_2H_2 hydrogenation step on bare and Ni doped $CeO_2(110)$ proceeds with the hydride.

3.3 C_2H_2 hydrogenation on bare and Ni doped $CeO_2(110)$

As stated above, on $CeO_2(110)$-O_v, the (Ce^{3+}-Ce^{4+})/O quasi-FLP facilitates H_2 dissociation via a heterolytic path. C_2H_2 hydrogenation should hence proceed with the resulting Ce-H hydride and O-H groups, similar to the reaction path on $CeO_2(111)$.[23] The corresponding energetics of the hydrogenation step are listed in Table 1 and geometries displayed in Figure 3 (a)-(f).

Before reaction, C_2H_2 weakly adsorbed on the surface with an adsorption energy of –0.38 eV. The adsorbed C_2H_2 species first reacts with H of the Ce-H hydride to form a weakly adsorbed C_2H_3 species (denoted as C_2H_3* (1)) (Figure 3(c)) by releasing 0.03 eV of energy. The calculated barrier of this hydrogenation step is 0.43 eV. Then, C_2H_3* (1) moves to a more stable adsorption state (C_2H_3* (Ce) in Figure 3(d)) by binding strongly to both Ce1 and Ce2 with the C1-Ce1 and C1-Ce2 distances of 2.93 and 2.94 Å, respectively. The adsorption energy of C_2H_3* (Ce) is –1.74 eV. It can directly react with the H on O1 to form C_2H_4 (Figure 3 (f)) by overcoming a barrier of 0.32 eV. The hydrogenation process is very similar to that on the bi-Ce^{3+}/O FLP of $CeO_2(110)$-$2O_v$. However, the barrier (0.32 eV) of the second hydrogenation step is about 0.26 eV lower than that (0.58 eV) on the bi-Ce^{3+}/O FLP of $CeO_2(110)$-$2O_v$.[19] As a result, for $CeO_2(110)$-O_v, the rate-determining step is the addition of the first hydrogen, while for $CeO_2(110)$-$2O_v$,[19] it is the addition of the second hydrogen. This might be due to the fact that on $CeO_2(110)$-$2O_v$, the Ce in Ce/O FLP is more exposed than that on $CeO_2(110)$-O_v. On Ni-$CeO_2(110)$-O_v, the hydrogenation of C_2H_2 also starts from the heterolytic products. The calculated reaction and activation energies are also shown in Table 1 and the corresponding geometries displayed in Figure 3 (g)-(l). C_2H_2 physisorption on Ni-$CeO_2(110)$-O_v has a binding energy of –0.49 eV. The weakly adsorbed C_2H_2 (Figure 3 (g)) is first hydrogenated by the hydride H, producing a weakly adsorbed C_2H_3 (C_2H_3*(1), (Figure 3(i)). This step releases an energy of 0.74 eV with a barrier of 0.28 eV. Before further hydrogenation, it transforms to a more stable adsorption state of C_2H_3* (Ce) (Figure 3(j)) with the

adsorption energy of –1.19 eV and with a C1-Ce1 distance of 2.55 Å. Finally, C_2H_3* (Ce) reacted with H bound to O to form C_2H_4 by overcoming a minor barrier of 0.07 eV, which is much lower than that (0.32 eV) on $CeO_2(110)$-O_v. This can be explained by the smaller adsorption energy of C_2H_3 (Ce) on the mono-Ce^{4+}/O FLP (–1.19 eV) than that on the (Ce^{3+}-Ce^{4+})/O quasi-FLP (–1.74 eV).

On Ni-$CeO_2(110)$-$2O_v$, the reaction and activation energies for the C_2H_2 hydrogenation are given in Table 1 and the geometries of the stationary points are shown in Figure 4. C_2H_2 is first adsorbed on the surface of Ni-$CeO_2(110)$-$2O_v$ with the C1-Ce1, C2-Ce1 and C2-H1 distances of 3.14, 3.18 and 3.25 Å and with the adsorption energy of –0.61 eV. The adsorbed C_2H_2 then reacts with the hydride H to form C_2H_3*(Ce) by overcoming a barrier of 0.40 eV, which is very similar to that on $CeO_2(110)$-O_v, but 0.12 eV higher than that on Ni-$CeO_2(110)$-O_v. In contrast to the cases on $CeO_2(110)$-O_v and Ni-$CeO_2(110)$-O_v, on Ni-$CeO_2(110)$-$2O_v$, the intermediate C_2H_3* (Ce) is directly formed via the reaction of C_2H_2* with the H adsorbed on Ce1. Finally, C_2H_3*(Ce) abstracts the H adsorbed on O producing C_2H_4* with a barrier of 0.32 eV, which is 0.25 eV higher than that on Ni-$CeO_2(110)$-O_v but is same as that (0.32 eV) on $CeO_2(110)$-O_v. The results indicates that the reduction of Ce^{4+} to Ce^{3+} in the mono-Ce/O FLP increases the barrier of first and second hydrogenation step.

The calculated energy profiles of C_2H_2 hydrogenation on $CeO_2(110)$-O_v, Ni-$CeO_2(110)$-O_v and Ni-$CeO_2(110)$-$2O_v$ are shown in Figure 5. To compare the catalytic activities of $CeO_2(110)$ and $CeO_2(111)$, the energy profiles of bare and Ni doped $CeO_2(111)$ surfaces with one oxygen vacancy ($CeO_2(111)$-O_v and Ni-$CeO_2(111)$-O_v) are also included in the same figure. For H_2 dissociation, on $CeO_2(110)$-O_v and Ni-$CeO_2(110)$-$2O_v$, the barrier (about 0.1 eV) is significantly lower than that (about 0.5 eV) on $CeO_2(111)$-O_v and Ni-$CeO_2(111)$-O_v. Even for Ni-$CeO_2(110)$-

O_v, the barrier (0.41 eV) is about 0.1 eV lower than that on $CeO_2(111)$-O_v and Ni-$CeO_2(111)$-O_v. The results indicate a higher efficiency of $CeO_2(110)$ for H_2 dissociation than $CeO_2(111)$. For the first hydrogenation step, the barriers on $CeO_2(110)$-O_v (0.43 eV), Ni-$CeO_2(110)$-$2O_v$ (0.40 eV), and $CeO_2(111)$-O_v (0.37 eV) are very close to each other, but higher than those on Ni-$CeO_2(110)$-O_v (0.28 eV) and Ni-$CeO_2(111)$-O_v (0.13 eV). This difference suggests that the barrier of first hydrogenation step is closely related to the oxidation state of Ce since on $CeO_2(110)$-O_v (0.43 eV), Ni-$CeO_2(110)$-$2O_v$ and $CeO_2(111)$-O_v, the Ce^{3+} takes part in forming Ce/O FLPs while on Ni-$CeO_2(110)$-O_v and Ni-$CeO_2(111)$-O_v, Ce^{4+} is in the Ce/O FLPs. For the second hydrogenation step, the barriers on $CeO_2(110)$-O_v (0.32 eV), Ni-$CeO_2(110)$-O_v (0.07 eV) and Ni-$CeO_2(110)$-$2O_v$ (0.32 eV) are all much lower than the those on $CeO_2(111)$-O_v (0.70 eV) and Ni-$CeO_2(111)$-O_v (0.62 eV), showing that the second hydrogenation step strongly depends on the surface structure. Judging from the rate-determining barrier, it found that on bare and doped $CeO_2(110)$, the barrier (about 0.4 eV) is about 0.2 eV lower than that on bare (0.70 eV) and doped (0.62 eV) $CeO_2(111)$. Thus, $CeO_2(110)$ is more active than $CeO_2(111)$ for acetylene hydrogenation, consistent with the experimental study.[14]

On $CeO_2(110)$-O_v/Ni-$CeO_2(110)$-$2O_v$, the barrier of first hydrogenation step (0.43/0.40 eV) is not only higher than that of the second hydrogenation step (0.32/0.32 eV), but also higher than that (0.12/0.13 eV) of H_2 dissociation. Thus, for $CeO_2(110)$-O_v and Ni-$CeO_2(110)$-$2O_v$, the first hydrogenation step is likely to control the reaction rate. While for Ni-$CeO_2(110)$-O_v, the barrier (0.41 eV) of H_2 dissociation is higher than that (0.28 eV) of the first hydrogenation step and that (0.07 eV) of second hydrogenation step, so that H_2 dissociation becomes the rate-determining step. The change of rate-determining step may be related to the different types of Ce species involved

in the active sites (FLPs) since in $CeO_2(110)$-O_v and Ni-$CeO_2(110)$-$2O_v$, it is Ce^{3+} that is involved in the Ce/O FLPs, while on Ni-$CeO_2(110)$-O_v, it is Ce^{4+} participating in the Ce/O FLPs.

In order to understand the effect of Ce on the activities of Ce/O FLPs, the density of states (DOSs) of $CeO_2(110)$-O_v, Ni-$CeO_2(110)$-O_v and Ni-$CeO_2(110)$-$2O_v$ were calculated and shown in Figure 6. The corresponding total and partial DOSs of O and Ce forming FLPs are given in the left and right panels, respectively. The results suggest that the total and partial DOSs of O 2*p* are very similar. However, comparing the results of Ce 4*f* states, it is found that there is a peak in the range from –2 to 0 eV for Ce1/Ce1 of $CeO_2(110)$-O_v/Ni-$CeO_2(110)$-$2O_v$, while no peak is observed in this range for Ce1 of Ni-$CeO_2(110)$-O_v. The closer to the Fermi level, the more active are Ce 4*f* valence electrons states. Thus, it can be expected that the Ce^{3+} in $CeO_2(110)$-O_v and Ni-$CeO_2(110)$-$2O_v$ would have stronger interaction with H and C_2H_3. It is confirmed by the larger adsorption energy of H and C_2H_3 on Ce in $CeO_2(110)$-O_v (–1.88 eV for H, –1.84 eV for C_2H_3) and in Ni-$CeO_2(110)$-$2O_v$ (–1.69 eV for H, –1.60 eV for C_2H_3) than that in Ni-$CeO_2(110)$-O_v (–1.22 eV for H and –1.19 eV for C_2H_3). The stronger interaction between Ce and H leads to higher activities for H_2 dissociation, resulting in lower barriers than those of the first hydrogenation step. Furthermore, the stronger adsorption of C_2H_3 presumably leads to higher barriers of the second hydrogenation step.

4. Conclusions

In this work, H_2 dissociation and C_2H_2 hydrogenation on bare and Ni doped $CeO_2(110)$ surfaces were investigated using the density functional theory. For $CeO_2(110)$, the endothermic formation of one O_v creates a (Ce^{3+}-Ce^{4+})/O quasi-FLP. Ni doping leads to the exothermic formation of first O_v and the easier generation of second O_v. On Ni-$CeO_2(110)$-O_v and Ni-$CeO_2(110)$-$2O_v$, one Ce and a non-adjacent O form a Ce^{4+}/O FLP and a Ce^{3+}/O FLP, respectively.

It is found that both the (Ce^{3+}-Ce^{4+})/O quasi-FLP and Ce/O FLP can promote the heterolytic dissociation of H_2 and hydrogenation of acetylene by the heterolytic products of Ce-H and O-H species.

For the (Ce^{3+}-Ce^{4+})/O quasi-FLP and Ce^{3+}/O FLP, the rate-determining step is the addition of the first hydrogen with a barrier of 0.43 and 0.40 eV, respectively. With the Ce^{4+}/O FLP of Ni-CeO_2(110)-O_v, on the other hand, the slowest step is the H_2 dissociation with a barrier of 0.41 eV. The change of rate-determining step can be attributed to the variation of the oxidation state of Ce. The Ce^{3+} species has a stronger interaction with adsorbates, leading to a higher activity for H_2 dissociation but increasing the barriers of first and second hydrogenation steps. As a result, the reduction of Ce in the Ce/O FLP enhances the activity of H_2 dissociation but suppresses the addition of first and second hydrogen, thus leading to the changes of rate-determining step. Moreover, our result reveals that the hydrogenation activity is strongly affected by the crystal facet. Both the bare and doped CeO_2(110) show a much lower rate-determining barrier than their CeO_2(111)) counterparts, confirming higher activity of CeO_2(110) than CeO_2(111) for acetylene hydrogenation, which is consistent with experimental observations. The results provide useful insights in developing effective catalysts.

Acknowledgements:

This work was supported by the National Natural Science Foundation of China (Grant no. 21962007 to S.Z., and 21973013 to S.L.), Natural Science Foundation of Jiangxi Province (Grant no. 2020BABL203009 to S.Z.), Foundation of Jiangxi Educational Committee (Grant no. GJJ190697 to S.Z.), and Qishan Scholarship Program of Fuzhou University (Grant no. XRC-17055 to S.L.), the National Natural Science Foundation of Fujian Province, China (Grant no.

2020J02025 to S.L.), and the "Chuying Program" for the Top Young Talents of Fujian Province.

H.G. acknowledges the support from the National Science Foundation (Grant no. CHE-1951328).

References

1 G. C. Bond, *Metal-catalysed reactions of hydrocarbons*, Springer, **2005**, p.
2 B. Bridier, N. Lopez and J. Perez-Ramirez, *Dalton Trans.* 2010, *39*, 8412-8419.
3 D. Teschner, J. Borsodi, A. Wootsch, Z. Révay, M. Hävecker, A. Knop-Gericke, S. D. Jackson and R. Schlögl, *Science* 2008, *320*, 86-89.
4 M. Crespo-Quesada, F. Cárdenas-Lizana, A.-L. Dessimoz and L. Kiwi-Minsker, *ACS Catal.* 2012, *2*, 1773-1786.
5 T. Mitsudome and K. Kaneda, *Green Chem.* 2013, *15*, 2636-2654.
6 J. Moon, Y. Cheng, L. L. Daemen, M. Li, F. Polo-Garzon, A. J. Ramirez-Cuesta and Z. Wu, *ACS Catal.* 2020, *10*, 5278-5287.
7 J. Kammert, J. Moon and Z. Wu, *Chin. J. Catal* 2020, *41*, 901-914.
8 X. Huang, K. Zhang, B. Peng, G. Wang, M. Muhler and F. Wang, *ACS Catal.* 2021, *11*, 9618-9678.
9 T. Montini, M. Melchionna, M. Monai and P. Fornasiero, *Chem. Rev.* 2016, *116*, 5987-6041.
10 Z. Zhang, Z.-Q. Wang, Z. Li, W.-B. Zheng, L. Fan, J. Zhang, Y.-M. Hu, M.-F. Luo, X.-P. Wu, X.-Q. Gong, W. Huang and J.-Q. Lu, *ACS Catal.* 2020, *10*, 14560-14566.
11 S. Zhang, Z.-Q. Huang, Y. Ma, W. Gao, J. Li, F. Cao, L. Li, C.-R. Chang and Y. Qu, *Nat. Commun.* 2017, *8*, 15266.
12 G. Vilé, B. Bridier, J. Wichert and J. Pérez-Ramírez, *Angew. Chem. Int. Ed.* 2012, *51*, 8620-8623.
13 G. Vilé, S. Colussi, F. Krumeich, A. Trovarelli and J. Pérez-Ramírez, *Angew. Chem. Int. Ed.* 2014, *53*, 12069-12072.
14 T. Cao, R. You, Z. Li, X. Zhang, D. Li, S. Chen, Z. Zhang and W. Huang, *Appl. Surf. Sci.* 2020, *501*, 144120.
15 T. Cao, R. You, X. Zhang, S. Chen, D. Li, Z. Zhang and W. Huang, *Phys. Chem. Chem. Phys.* 2018, *20*, 9659-9670.
16 K. Werner, X. Weng, F. Calaza, M. Sterrer, T. Kropp, J. Paier, J. Sauer, M. Wilde, K. Fukutani, S. Shaikhutdinov and H.-J. Freund, *J. Am. Chem. Soc.* 2017, *139*, 17608-17616.
17 C. Riley, A. De La Riva, S. Zhou, Q. Wan, E. Peterson, K. Artyushkova, M. D. Farahani, H. B. Friedrich, L. Burkemper, N.-V. Atudorei, S. Lin, H. Guo and A. Datye, *ChemCatChem* 2019, *11*, 1526-1533.
18 J. Carrasco, G. Vilé, D. Fernández-Torre, R. Pérez, J. Pérez-Ramírez and M. V. Ganduglia-Pirovano, *J. Phys. Chem. C* 2014, *118*, 5352-5360.
19 Z.-Q. Huang, L.-P. Liu, S. Qi, S. Zhang, Y. Qu and C.-R. Chang, *ACS Catal.* 2018, *8*, 546-554.
20 G. Vilé, P. Dähler, J. Vecchietti, M. Baltanás, S. Collins, M. Calatayud, A. Bonivardi and J. Pérez-Ramírez, *J. Catal.* 2015, *324*, 69-78.
21 M. García-Melchor, L. Bellarosa and N. López, *ACS Catal.* 2014, *4*, 4015-4020.
22 S. Zhou, L. Gao, F. Wei, S. Lin and H. Guo, *J. Catal.* 2019, *375*, 410-418.
23 C. Riley, S. Zhou, D. Kunwar, A. De La Riva, E. Peterson, R. Payne, L. Gao, S. Lin, H. Guo and A. Datye, *J. Am. Chem. Soc.* 2018, *140*, 12964-12973.
24 D. W. Stephan, *J. Am. Chem. Soc.* 2015, *137*, 10018-10032.
25 D. W. Stephan, *Acc. Chem. Res.* 2014, *48*, 306-316.
26 H. Lee, Y. N. Choi, D.-W. Lim, M. M. Rahman, Y.-I. Kim, I. H. Cho, H. W. Kang, J.-H. Seo, C. Jeon and K. B. Yoon, *Angew. Chem. Int. Ed.* 2015, *54*, 13080-13084.
27 X. Sun, B. Li, T. Liu, J. Song and D. S. Su, *Phys. Chem. Chem. Phys.* 2016, *18*, 11120-11124.

28 K. K. Ghuman, L. B. Hoch, T. E. Wood, C. Mims, C. V. Singh and G. A. Ozin, *ACS Catal.* 2016, *6*, 5764-5770.
29 Z. Chen, J. Zhao, J. Zhao, Z. Chen and L. Yin, *Nanoscale* 2019, *11*, 20777-20784.
30 J. Zhao, X. Liu and Z. Chen, *ACS Catal.* 2017, *7*, 766-771.
31 Q. Wan, J. Li, R. Jiang and S. Lin, *Phys. Chem. Chem. Phys.* 2021, *23*, 24349-24356.
32 Z. Wu, Y. Cheng, F. Tao, L. Daemen, G. S. Foo, L. Nguyen, X. Zhang, A. Beste and A. J. Ramirez-Cuesta, *J. Am. Chem. Soc.* 2017, *139*, 9721-9727.
33 Z. Li, K. Werner, K. Qian, R. You, A. Płucienik, A. Jia, L. Wu, L. Zhang, H. Pan, H. Kuhlenbeck, S. Shaikhutdinov, W. Huang and H.-J. Freund, *Angew. Chem. Int. Ed.* 2019, *58*, 14686-14693.
34 J. Paier, C. J. Nelin, P. S. Bagus, A. Plucienik, H. Kuhlenbeck and H.-J. Freund, *J. Electron. Spectrosc. Relat. Phenom.* 2021, 147088.
35 J. Song, Z.-F. Huang, L. Pan, J.-J. Zou, X. Zhang and L. Wang, *ACS Catal.* 2015, *5*, 6594-6599.
36 D. Albani, M. Capdevila-Cortada, G. Vilé, S. Mitchell, O. Martin, N. López and J. Pérez-Ramírez, *Angew. Chem. Int. Ed.* 2017, *56*, 10755-10760.
37 M. S. Frei, M. Capdevila-Cortada, R. García-Muelas, C. Mondelli, N. López, J. A. Stewart, D. Curulla Ferré and J. Pérez-Ramírez, *J. Catal.* 2018, *361*, 313-321.
38 W.-H. Feng, M.-M. Yu, L.-J. Wang, Y.-T. Miao, M. Shakouri, J. Ran, Y. Hu, Z. Li, R. Huang, Y.-L. Lu, D. Gao and J.-F. Wu, *ACS Catal.* 2021, *11*, 4704-4711.
39 Q. Wan, Y. Chen, S. Zhou, J. Lin and S. Lin, *J. Mater. Chem. A* 2021, *9*, 14064-14073.
40 A. Trovarelli and J. Llorca, *ACS Catal.* 2017, *7*, 4716-4735.
41 F. Jiang, S. Wang, B. Liu, J. Liu, L. Wang, Y. Xiao, Y. Xu and X. Liu, *ACS Catal.* 2020, *10*, 11493-11509.
42 X. Zhang, R. You, D. Li, T. Cao and W. Huang, *ACS Appl. Mater. Interfaces* 2017, *9*, 35897-35907.
43 Z. Hu, X. Liu, D. Meng, Y. Guo, Y. Guo and G. Lu, *ACS Catal.* 2016, *6*, 2265-2279.
44 J. Han, J. Meeprasert, P. Maitarad, S. Nammuangruk, L. Shi and D. Zhang, *J. Phys. Chem. C* 2016, *120*, 1523-1533.
45 O. Matz and M. Calatayud, *ACS Omega* 2018, *3*, 16063-16073.
46 Z.-Q. Wang, D.-R. Chu, H. Zhou, X.-P. Wu and X.-Q. Gong, *ACS Catal.* 2022, *12*, 624-632.
47 M. García-Melchor and N. López, *J. Phys. Chem. C* 2014, *118*, 10921-10926.
48 W. Zhang, M. Pu and M. Lei, *Langmuir* 2020, *36*, 5891-5901.
49 J. Paier, C. Penschke and J. Sauer, *Chem. Rev.* 2013, *113*, 3949-3985.
50 Y. Irene and N. Michael, *J. Phys.: Condens. Matter* 2010, *22*, 135004.
51 M. Nolan, *J. Mater. Chem.* 2011, *21*, 9160-9168.
52 M. Nolan, *J. Phys. Chem. C* 2011, *115*, 6671-6681.
53 W. Q. Li, S. Goverapet Srinivasan, D. R. Salahub and T. Heine, *Phys. Chem. Chem. Phys.* 2016, *18*, 11139-11149.
54 G. Kresse and J. Furthmüller, *Phys. Rev. B* 1996, *54*, 11169-11186.
55 G. Kresse and J. Furthmüller, *Comput. Mater. Sci.* 1996, *6*, 15-50.
56 J. P. Perdew, K. Burke and M. Ernzerhof, *Phys. Rev. Lett.* 1996, *77*, 3865-3868.
57 S. Grimme, J. Antony, S. Ehrlich and H. Krieg, *J. Chem. Phys.* 2010, *132*, 154104.
58 P. E. Blöchl, *Phys. Rev. B* 1994, *50*, 17953-17979.
59 M. D. Krcha and M. J. Janik, *Int. J. Quantum Chem.* 2014, *114*, 8-13.
60 E. W. McFarland and H. Metiu, *Chem. Rev.* 2013, *113*, 4391-4427.
61 S. Fabris, G. Vicario, G. Balducci, S. de Gironcoli and S. Baroni, *J. Phys. Chem. B* 2005, *109*, 22860-22867.
62 G. Henkelman, B. P. Uberuaga and H. Jónsson, *J. Chem. Phys.* 2000, *113*, 9901-9904.
63 D. W. Stephan and G. Erker, *Angew. Chem. Int. Ed.* 2010, *49*, 46-76.
64 Y. Ma, S. Zhang, C.-R. Chang, Z.-Q. Huang, J. C. Ho and Y. Qu, *Chem. Soc. Rev.* 2018, *47*, 5541-5553.
65 Z.-Q. Huang, T. Zhang, C.-R. Chang and J. Li, *ACS Catal.* 2019, *9*, 5523-5536.

Table 1 Reaction energies (ΔE) and activation energies (E_a) for the elementary steps involved in the H_2 dissociation and C_2H_2 hydrogenation on $CeO_2(110)$-O_v, Ni-$CeO_2(110)$-O_v and Ni-$CeO_2(110)$-$2O_v$. Here I, III, IV, VI, VII, IX denote the states indicated in Figure 5.

Reactions	$CeO_2(110)$-O_v		Ni-$CeO_2(110)$-O_v		Ni-$CeO_2(110)$-$2O_v$	
	ΔE	E_a	ΔE	E_a	ΔE	E_a
H_2+*→H_2* (I)	–0.27	-	–0.21	-	–0.22	-
H_2*→H*(O) +H*(Ce) (III)	–0.24	0.12	0.23	0.41	–0.00	0.13
H*(O)+H*(Ce) →2H* (O)	–1.63	1.06	–2.59	0.73	–2.26	1.14
C_2H_2(g)+2H*+*→C_2H_2*+2H* (IV)	–0.38	-	–0.49	-	–0.81	-
C_2H_2*+2H*→C_2H_3*(Ce)+H* (VII)	-	-	-	-	–1.29	0.40
C_2H_2*+2H*→C_2H_3* (1) +H* (VI)	–0.03	0.43	–0.90	0.28	-	-
C_2H_3* (1) +H*→C_2H_3 *(Ce)+H* (VII)	–1.33	-	–0.45	-	-	-
C_2H_3*(Ce)+H*→C_2H_4* (IX)	–0.63	0.32	–1.09	0.07	–0.68	0.32

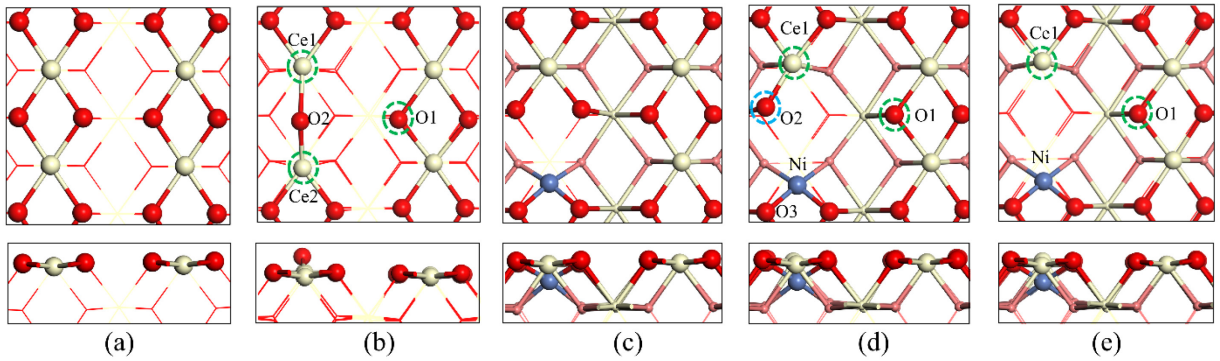

Figure 1. Top and side views of (a) $CeO_2(110)$, (b) $CeO_2(110)$-O_v, (c) Ni-$CeO_2(110)$, (d) Ni-$CeO_2(110)$-O_v and Ni-$CeO_2(110)$-$2O_v$. On $CeO_2(110)$-O_v, the two Ce and one O atoms in green circles form a Ce^{3+}-Ce^{4+}/O quasi-FLP. On Ni-$CeO_2(110)$-O_v and Ni-$CeO_2(110)$-$2O_v$, the Ce and O atoms in green circles form the mono-Ce/O FLPs. On Ni-$CeO_2(110)$-O_v, the O2 in blue circle and Ce1 in green circles make a CLP. Color scheme: Ni, blue; Ce, yellow; oxygen, red; subsurface oxygen, light red.

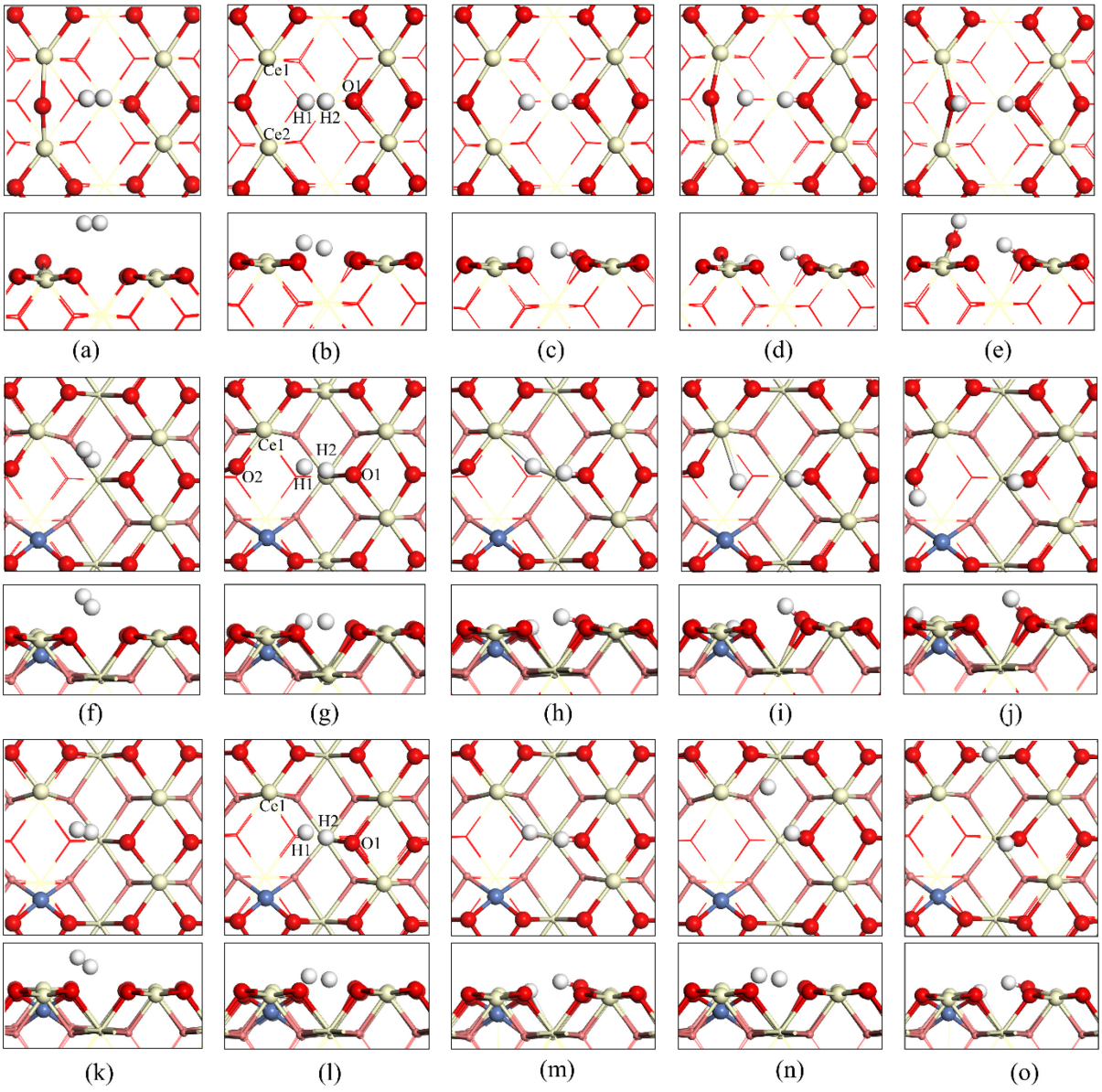

Figure 2. Top and side views of (a) H_2 adsorption (H_2*) (I), (b) TS of the H_2 dissociation (II), (c) heterolytic products (H*–Ce + H*–O) (III), (d) TS of H*−Ce migration, (e) homolytic products (H*–O + H*–O) on CeO_2(110)-O_v, (f) H_2 adsorption (H_2*) (I), (g) TS of H_2 dissociation (II), (h) heterolytic product (H*–Ce + H*–O) (III), (i) TS for H* migration from Ce to O, (j) homolytic product (H*–O + H*–O) on Ni@CeO_2(110)-O_v, (k) H_2 adsorption (H_2*) (I), (l) TS of H_2 dissociation (II), (m) heterolytic product (H*–Ce + H*–O) (III), (n) TS for H* migration from Ce to O, and (o) homolytic product (H*–O + H*–O) on Ni@CeO_2(110)-2O_v. Here, I, II and III denote the states indicated in Figure 5. Color scheme: Ni, blue; Ce, yellow; surface O, red; subsurface O, light red; H, white.

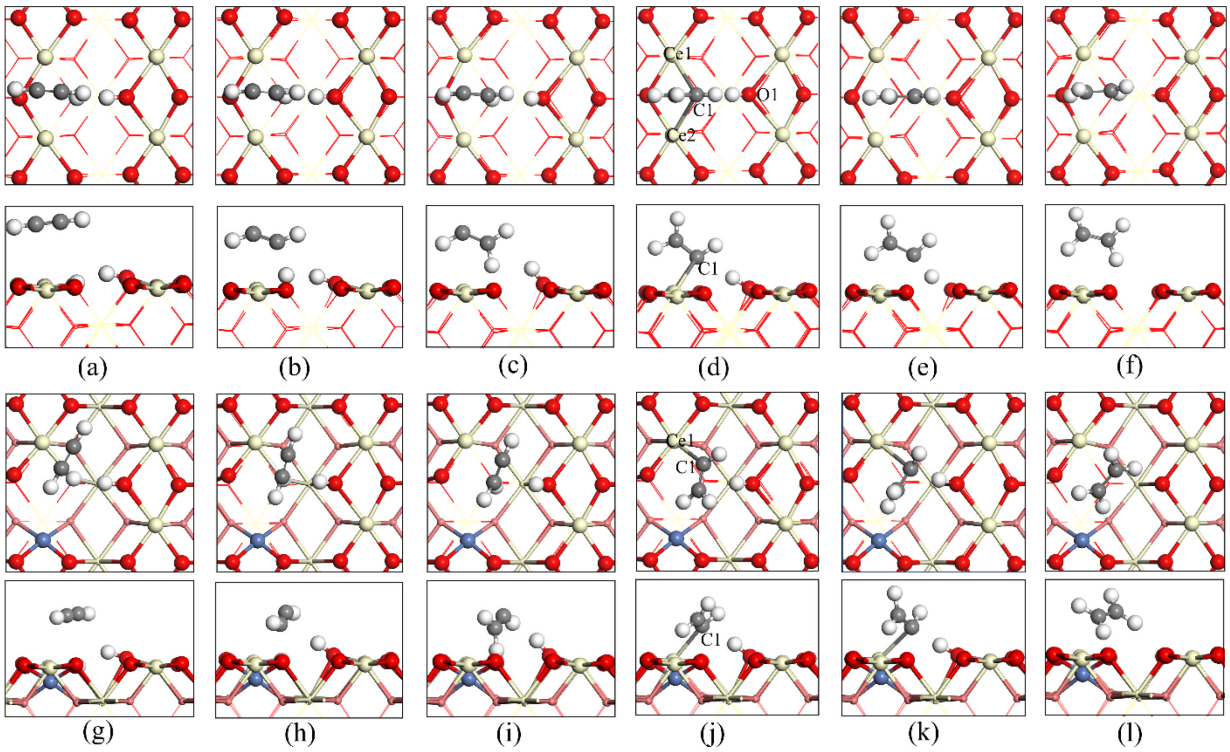

Figure 3. Top and side views of (a) 2H* + C_2H_2* (IV), (b) TS for first hydrogenation step (V), (c) H* + C_2H_3*(1) (VI), (d) H* + C_2H_3* (Ce) (VII), (e) TS for second hydrogenation step (VIII), and (f) C_2H_4* (IX) on CeO_2(110)-O_v; (g) 2H* + C_2H_2*(IV), (h) TS for first hydrogenation step (V), (i) H* + C_2H_3* (1) (VI), (j) H* + C_2H_3*(Ce) (VII), (k) TS for second hydrogenation step (VIII) and (l) C_2H_4* (IX) on Ni-CeO_2(110)-O_v. Here, IV, V, VI, VII, VIII and IX denote the states indicated in Figure 5. Color scheme: Ni, blue; Ce, yellow; surface O, red; subsurface O, light red; H, white; C, grey.

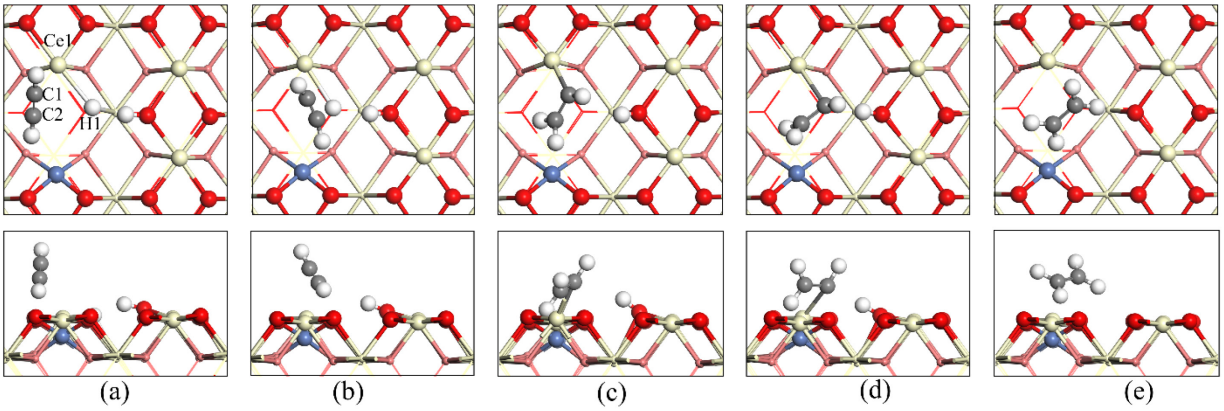

Figure 4. Top and side views of (a) 2H* + C_2H_2*(IV), (b) TS for first hydrogenation step (V), (c) H* + C_2H_3*(Ce) (VII), (d) TS for second hydrogenation step (VIII) and (e) C_2H_4* (IX) on Ni-CeO_2(110)-$2O_v$. Here, IV, V, VII, VIII and IX denote the states indicated in Figure 5. Color scheme: Ni, blue; Ce, yellow; surface O, red; subsurface O, light red; H, white; C, grey.

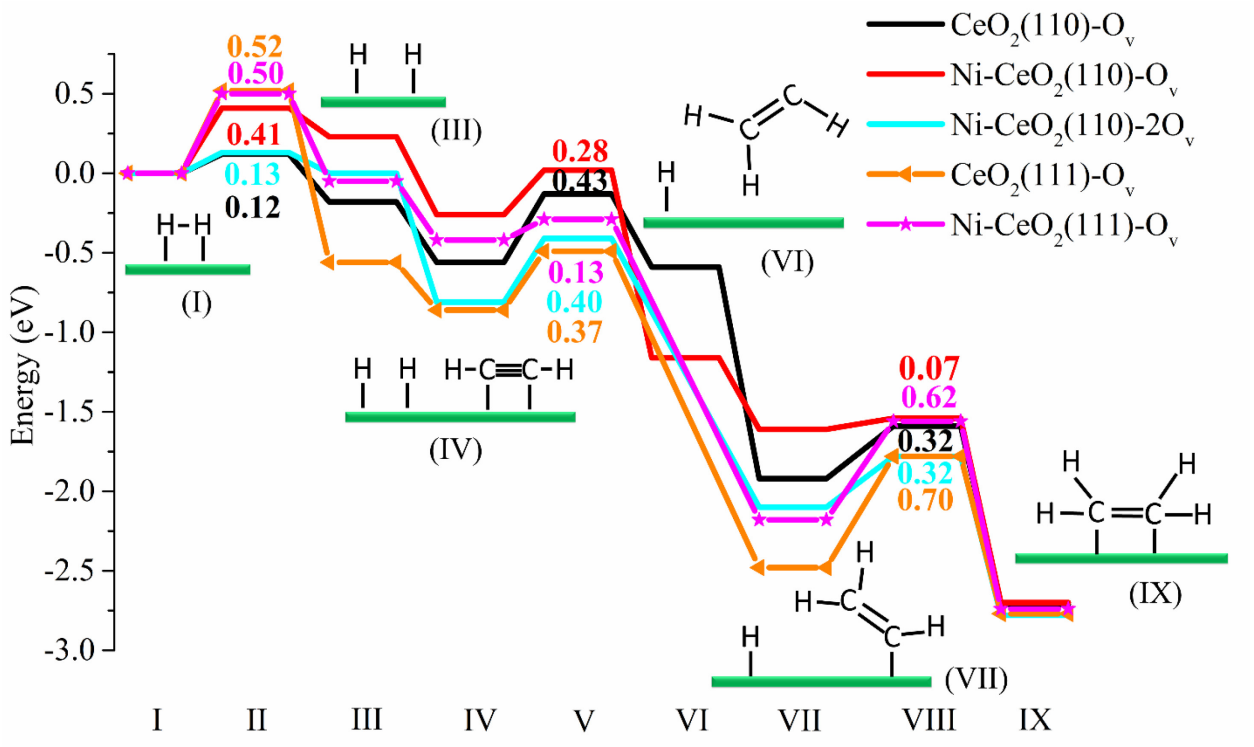

Figure 5. Calculated energy profiles of C_2H_2 hydrogenation on $CeO_2(110)$-O_v, Ni-$CeO_2(110)$-O_v and Ni-$CeO_2(110)$-$2O_v$. The results for $CeO_2(111)$-O_v and Ni-$CeO_2(111)$-O_v are also given for comparison. The data given in the Figure indicate the activation energies (eV) of TSs. I: H_2*, II: TS for H_2 dissociation, III: 2H* (H*–O + H*–Ce), IV: C_2H_2* + 2H*, V: TS for first hydrogenation step; VI: H*+ C_2H_3*(1), VII: H* + C_2H_3* (Ce), VIII: TS for second hydrogenation step, IX: C_2H_4*. Here * denotes the adsorption state.

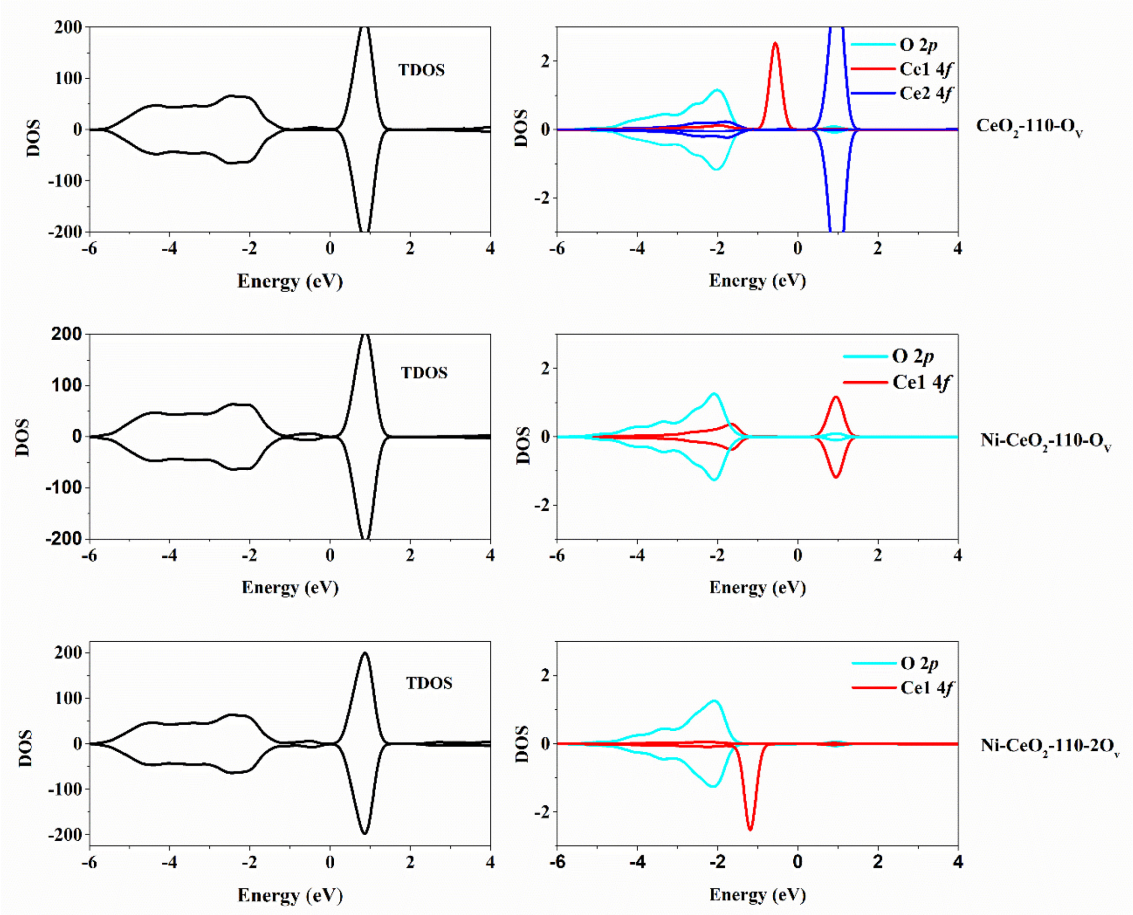

Figure 6. Total and partial densities of states of CeO_2(110)-O_v, Ni-CeO_2(110)-O_v and Ni-CeO_2(110)-$2O_v$.

Graphical abstract